Title
Identification of Photoacidic Behavior Using AC and Open-Circuit Photoelectrochemical Techniques

Journal
ECS Journal of Solid State Science and Technology, 11(10)

ISSN
2162-8769

Authors
Glancy, Jennifer
Luo, Simon
Kim, Tea-Yon
et al.

Publication Date
2022-10-01

DOI
10.1149/2162-8777/ac71ff

ECS Journal of Solid State Science and Technology, 2022 **11** 105002

Identification of Photoacidic Behavior Using AC and Open-Circuit Photoelectrochemical Techniques

Jennifer Glancy,[1] Simon Luo,[1] Tea-Yon Kim,[1] and Shane Ardo[1,2,3,z]

[1]*Department of Chemistry, University of California Irvine, Irvine, CA 92697, United States of America*
[2]*Department of Chemical & Biomolecular Engineering, University of California Irvine, Irvine, CA 92697, United States of America*
[3]*Department of Materials Science & Engineering, University of California Irvine, Irvine, CA 92697, United States of America*

Photoacids are molecules whose acidity increases through absorption of light. When the excited-state lifetime of a photoacid is sufficiently long, proton transfer from its thermally equilibrated electronic excited state results in a transient change in pH and/or pOH, which is commonly detected using spectroscopic techniques. Herein we expand this measurement toolkit by introducing alternating AC and open-circuit photoelectrochemical techniques that characterize photoacidic behavior from a model photoacid, the sodium salt of 8-hydroxypyrene-1,3,6-trisulfonate, dissolved in aqueous solutions in a thin-pathlength two-electrode cell. Continuous illumination of protonated photoacids in their electronic ground state results in significant and reproducible changes in low-frequency impedance and open-circuit potential. When these molecules are made to be non-acidic, via deprotonation using more alkaline pH conditions or methoxylation via synthesis, electrochemical data measured in the dark and under illumination are nearly identical. Best fits of AC electrochemical data to a simplified equivalent circuit support that photoelectrochemical responses are likely due to changes in local proton concentration at the electrode|electrolyte interface, and not changes in proton flux due to mass transfer, as previously suggested. Collectively, our results provide further insight into the utility of these photoelectrochemical techniques to probe photoacidic behavior.
 [DOI: 10.1149/2162-8777/ac71ff]

Manuscript submitted December 21, 2021; revised manuscript received May 11, 2022. Published October 6, 2022. *This paper is part of the JSS Focus Issue on Focus Issue In Honor of John Goodenough: A Centenarian Milestone.*

Supplementary material for this article is available online

Photoacids and photobases constitute a class of molecules that exhibit a reversible change in Brønsted–Lowry acidity upon absorption of light. Depending on the underlying mechanism of photoacidity/photobasicity, the cycle of light absorption, (de)protonation, and ultimate regeneration can occur over timescales that span up to 15 orders-of-magnitude in water alone.[1–5] For example, excited-state proton transfer occurs on timescales consistent with all excited-state photochemical processes, with time constants that are as fast as a bond vibration (hundreds of femtoseconds) to as slow as the lifetime of the electronic excited state (hundreds of nanoseconds).[6–9] Subsequent to excited-state proton transfer, ground-state regeneration occurs on timescales of up to hundreds of microseconds,[10,11] and photo-driven cis/trans isomerization leading to cyclization via covalent bond formation and deprotonation, followed by re-equilibration, occurs on timescales of up to minutes.[12–14] Because of these disparate timescales, techniques to measure photoacidic/photobasic behavior are quite varied. For slow photoinduced ground-state proton-transfer processes, such as those that involve making or breaking of strong covalent bonds, rather straightforward techniques exist that rely on quantifying pH changes either directly, using a standard pH probe, or indirectly, using electronic absorption spectroscopy to quantify the extent of (de) protonation of ground-state species.[14–18] Measuring photoacidity/photobasicity of excited-state species requires techniques with faster time resolution, such as time-resolved photoluminescence spectroscopy.[19] However, when emission quantum yields from excited-state molecules are so small that luminescence is undetectable experimentally, more advanced and less readily available techniques are required, such as ultrafast and nanosecond transient absorption spectroscopies. A more easily accessible and generally applicable technique to identify photoacidic/photobasic behavior would be useful.

Dawlaty and coworkers recently developed and utilized a photoelectrochemical impedance spectroscopy (photo-EIS) technique to quantitatively assess photoacidity of a well-known photoacid dye molecule, i.e. the sodium salt of 8-hydroxypyrene-1,3,6-trisulfonate (HPTS, pyranine; PTS–OH) (Fig. 1a), dissolved in an aqueous solution or impregnated in poly(ethylene glycol).[20] They reported that their technique sensed a steady-state change in the concentration of solvated protons under continuous illumination, suggesting they would have observed a decrease in bulk solution resistance. However, photoinduced changes in bulk solution resistance are challenging to measure because the solution is in series with other bulk resistances that can be significantly larger. For example, resistance due to electronic charge transport in the plane of the transparent-conductive-oxide electrodes is often rather large in comparison to resistance due to ionic charge transport across thin-pathlength aqueous electrolytes. Moreover, aqu-eous electrolytes used in these experiments have ionic strengths that are inherently quite large due to water-solubilizing charged groups present on most photoacids and their mobile counterions. As reported previously,[20] this means that continuous illumination elicits negligible changes in series resistance, even with effective photoacids/photobases and moderate illumination intensities.

Photoinduced changes in interfacial charge-transfer impedance and/or mass-transfer-limited impedance are in theory less challenging to measure, but require that protons and/or hydroxides be involved in interfacial charge-transfer reactions and that their concentration(s) are perturbed significantly near the electrode|electrolyte interface and/or within the diffusion layer of an electrode(s), respectively. The concentration of protons and/or hydroxides can be quite small and stable, e.g. ~10^{-7} M at pH 7, and can be perturbed significantly by illumination of a photoelectrochemical cell whose walls consist of transparent-conductive-oxide electrodes and that is filled with a solution of photoacids whose absorption profile follows the Beer–Lambert law. Doing so generates a larger number of excited-state molecules at one electrode *vs* the other electrode and therefore, as long as the potential of each electrode is sensitive to the

[z]E-mail: ardo@uci.edu

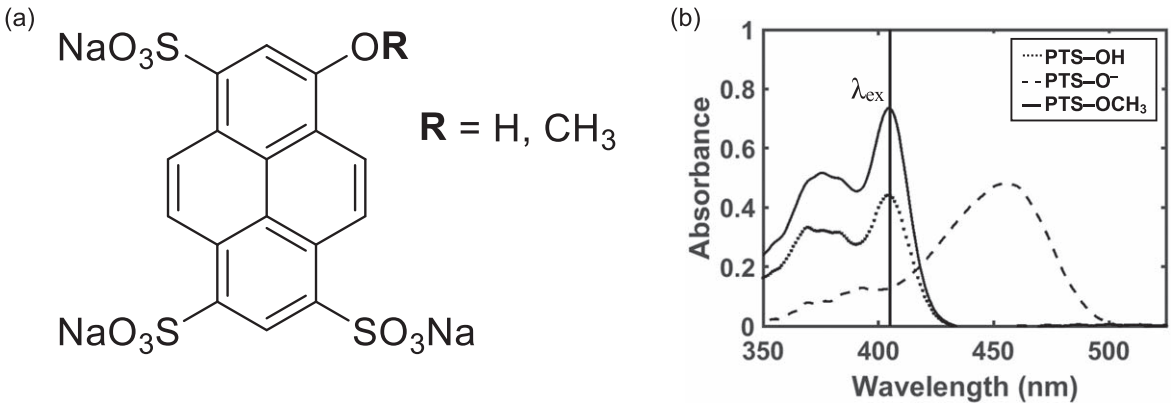

Figure 1. (a) Chemical structures of the sodium salts of 8-hydroxypyrene-1,3,6-trisulfonate (HPTS; PTS–OH; R = H) and 8-methoxypyrene-1,3,6-trisulfonate (PTS–OCH_3; R = CH_3). (b) Electronic absorption spectra of aqueous solutions of 1 mM sodium salts of protonated HPTS (PTS–OH), deprotonated HPTS (PTS–O^-), and methoxylated HPTS (PTS–OCH_3), each measured in a thin-pathlength cell, with a 250 μm thick spacer.

local concentration of protons and/or hydroxides, illumination should decrease the low-frequency impedance, as observed by Dawlaty and colleagues.[20] While best fits to their equivalent circuit suggested a *decrease* in the resistance for semi-infinite diffusion, unexpectedly it also suggested an *increase* in the resistance for interfacial charge transfer. To help clarify this result, herein we report data obtained from transient measurements of open-circuit potential and photo-EIS of aqueous solutions of PTS–OH in the dark and under illumination. We performed measurements at several pH values, because it is well-known that excitation into an electronic absorption transition of PTS–OH (Fig. 1b) dissolved in aqueous solution results in excited-state proton transfer[4,21–24] with near-unity quantum yield when pH 2–6 is used[25,26] since the pK_a value of PTS–OH decreases from ~7 in its electronic ground state to ~1 in its thermally-equilibrated electronic excited state.[19,23,27–30] We also compared these results to those from the methoxylated version of this photoacid that does not contain a protic group, PTS–OCH_3 (Fig. 1), which we synthesized using previously reported procedures[27] to serve as a negative control. Together, our data provide additional details of the processes that lead to the previously observed low-frequency photo-EIS response,[20] and further support that the response is due to a transient change in solvated proton activity.

Experimental

Chemicals.—The following chemicals were used without further purification from the indicated suppliers: hydrochloric acid (36.5% 38.0% w/w, Fisher Scientific), sodium hydroxide (>95%, Macron Fine Chemicals), sodium chloride (99.6%, Fisher Scientific), sodium 8-hydroxypyrene-1,3,6-trisulfonate (HPTS, pyranine; PTS–OH) (>95%, Carbosmith), iron(III) chloride (98%, anhydrous, Alfa Aesar), iron(II) chloride (99%, anhydrous, Acros Organics). Sodium 8-methoxy-pyrene-1,3,6-trisulfonate (PTS–OCH_3) was synthesized using iodomethane (99%, Alfa Aesar) and sodium hydroxide (>95%, Macron Fine Chemicals) according to a previously reported procedure.[27] Unless noted otherwise, solutions were made using deionized water, which resulted in reproducible photo-EIS data under illumination that changed monotonically over time until reaching a steady-state condition, whereas use of ultrapure water (Millipore Sigma, Milli-Q Reference Water Purification System) resulted in more erratic results.

Cell design.—Our cell was modeled after that used by Dawlaty and colleagues,[20] with several minor alterations (Fig. S1 (available online at stacks.iop.org/JSS/11/105002/mmedia)), and it was used to measure the open-circuit potential (E_{oc}) and EIS data in the dark and under illumination, as well as electronic absorption spectra. Briefly, our cell was constructed by modifying a thin-pathlength infrared spectroscopy liquid cell (Super-Sealed Liquid Cell, PIKE Technologies) using cell windows consisting of electrically conductive optically transparent fluorine-doped tin–oxide-coated glass (FTO) (Hartford Glass) electrodes separated by a 250 μm thick PTFE spacer, unless noted otherwise. Electrical connections to the external circuit were made by contacting the top edge of each FTO electrode with a copper wire via intervening silver paint and covering it with epoxy. For measurements comparing limited/confined diffusion with an absorbing *vs* reflecting finite boundary, one FTO electrode was partially etched to provide two separate counter electrodes that were each individually contacted with an alligator clip. Two 3/16 inch holes aligned with the injection ports of the cell housing were drilled into one FTO electrode to allow for introduction of aqueous photoacid solutions. Before cell assembly and between measurements, both FTO electrodes were thoroughly cleaned with ethanol and acetone and dried under a stream of N_2(g). After cell assembly and compression by tightening the screws of the cell, 150 μL of solution was injected to form a uniform layer that was visible across the entire cell window and showed no presence of air bubbles. The geometric area of the FTO electrodes wetted by aqueous electrolyte was 2.9 cm^2, and the circular opening for illumination was 1.3 cm^2 (1.3 cm in diameter).

Electronic absorption spectroscopy.—Electronic absorption spectra were acquired at room temperature using an ultraviolet–-visible absorption spectrophotometer (Cary 60, Agilent Technologies) with a spectral resolution of 1 nm. Electronic absorption spectra were measured by aligning the window of the cell perpendicular to the optical beam path, and spectra are reported *vs* a baseline spectrum taken on the cell filled with deionized water or ultrapure water, respective to the medium used as the solvent.

Photo-electrochemical impedance spectroscopy (Photo-EIS).—The cell was aligned in a homebuilt Faraday cage that contained a small opening to allow for illumination. Photo-EIS data were acquired in the dark and under continuous illumination using a two-electrode configuration with a DC applied potential bias equal to 0 V *vs* E_{oc} and sweeping over a frequency range of 10^{-1} to 10^6 Hz (4 points per decade and 10 mV AC potential amplitude), unless noted otherwise. Incident light was generated by a visible-light-emitting laser pointer (405 ± 10 nm), calibrated using a Si photodiode (FDS100, Thorlabs) to have a photon flux of 8.4×10^{15} photon s^{-1} and full-width-at-half-maximum beam diameter of 1.96 mm, which then passed through a beam expander to result in illumination that slightly underfilled the cell window to ensure near-maximum illumination of the aqueous electrolyte. Best fits of EIS data to an appropriate equivalent circuit were performed using EC-LAB Version 11.27 ZFit impedance fitting software from Bio-Logic

Science Instruments (Levenberg–Marquardt method with |Z| weighting and 5000 fitting iterations). Values of the bulk resistance, R_s, were fixed to those determined by linear extrapolation of the Nyquist plot to the real resistance *x*-axis.

Open-circuit potential (E_{oc}).—Herein we define open-circuit photovoltage (V_{oc}) as the change in E_{oc} under illumination. Measurements of V_{oc} in our cell were performed in alternation with each photo-EIS measurement, unless noted otherwise. The pH dependence of E_{oc} values for a single electrode was determined external to the cell using two pieces of FTO, as a working and counter electrode, and a saturated calomel electrode (SCE), as the reference electrode. These three electrodes were immersed in a beaker filled with solutions identical to those used for other electrochemical experiments.

Results and Discussion

Effects of light on Nyquist plots of electrochemical impedance spectroscopy data.—EIS data obtained in the dark and under continuous illumination are shown as Nyquist plots for 1 mM aqueous solutions of the sodium salts of photoacidic PTS–OH (Figs. 2a, 2b) and non-photoacidic PTS–O^- and PTS–OCH_3 (Figs. 2c, 2d). Protonated PTS–OH exhibited similar responses to light as those observed previously by Dawlaty and colleagues.[20] Changes in low-frequency impedance values are consistent with alterations in rates of interfacial charge-transfer reactions and/or fluxes of mass-transfer processes. As shown in Figs. 2c, 2d, when the pH was changed to a value where photoacids were deprotonated as PTS–O^-, or when a control dye containing no protic bonds was used as PTS–OCH_3 and at a similar pH value used with protonated PTS–OH, changes in photo-EIS data were significantly smaller. This suggests that a protic group and excited-state proton transfer are responsible for the majority of observed changes in low-frequency impedance, and that other processes such as excited-state electron transfer, local heating, and/or quenching by O_2 are not dominant.[31] Moreover, the extent of change in low-frequency impedance cannot be ascribed to differences in the rate of photon absorption (Fig. S2a), and notably, PTS–OCH_3 absorbed light at the excitation wavelength more strongly than any protonation state of the photoacid (Fig. 1b). Moreover, solutions containing other concentrations of PTS–OH and/or at other pH values between 2 and 6 (Fig. S3), or in the presence of excess salt (Fig. 2b), also exhibited a significant photo-EIS response. Collectively, our suite of measurements and resulting trends in photo-EIS data are consistent with observations made by Dawlaty and colleagues.[20] However, the mechanism for transducing changes in proton concentration to an electrochemical response remained uncertain, and therefore warranted further analysis.

Means by which photogenerated protons can influence electrochemical processes.—A change in the concentration of protons can affect various aspects of a membraneless aqueous electrochemical cell: bulk solution resistance, diffuse-layer capacitance near an electrode|electrolyte interface, and proton-coupled redox reactivity at an electrode|electrolyte interface, either due to changes in mass action or mass transfer. Therefore, we performed a series of measurements to assess which of these processes dominated observed changes in EIS data when illuminated.

Bulk solution resistance is inversely proportional to the ionic conductivity, which is directly related to the weighted sum of the ion

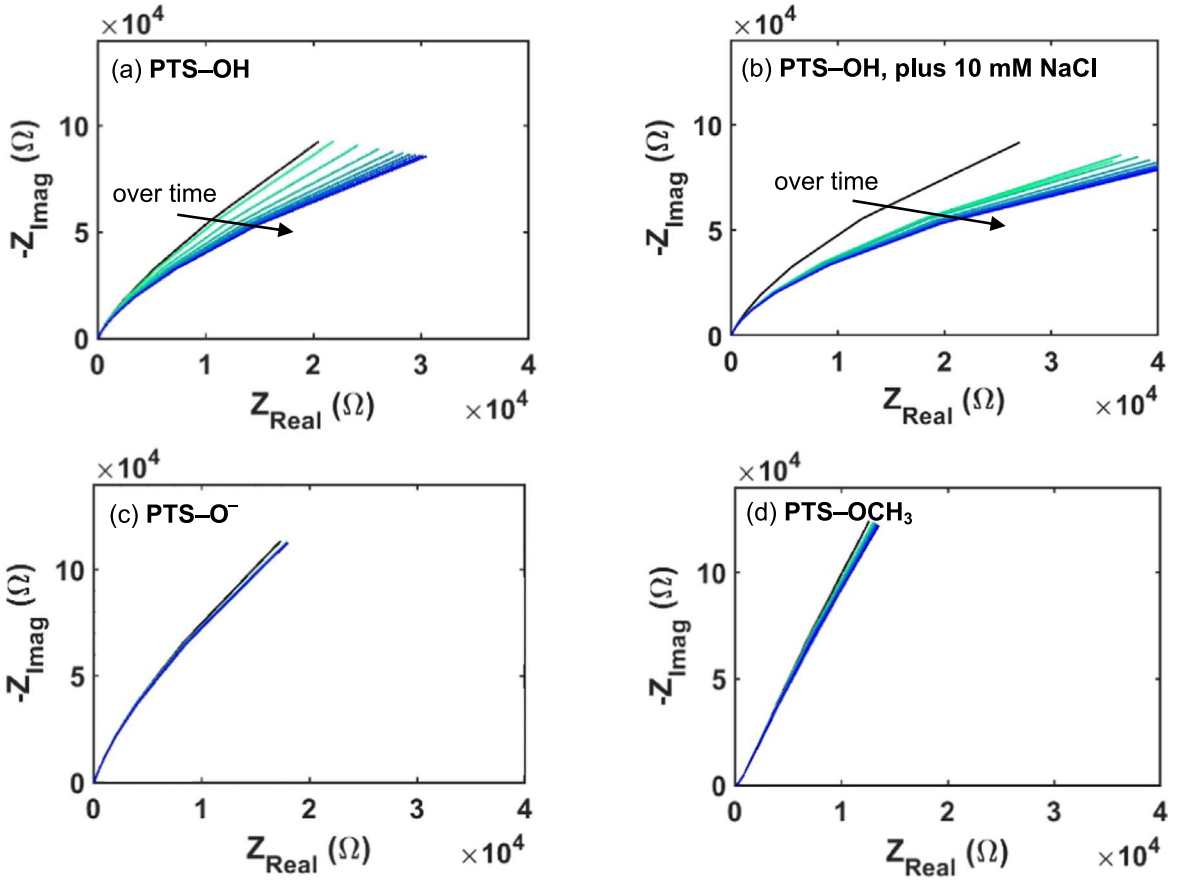

Figure 2. Two-electrode EIS data measured over time between two nominally identical FTO electrodes in a thin-pathlength cell, with a 250 μm thick spacer, and shown as Nyquist plots for 1 mM aqueous solutions of the sodium salt of (a) PTS–OH (pH 4.2), (b) PTS–OH (pH 4.0, 10 mM NaCl(aq)), (c) PTS–O^- (pH 9.7, from addition of approximately equimolar NaOH), and (d) PTS–OCH_3 (pH 3.7). The Nyquist plots include EIS data measured initially in the dark (black) and photo-EIS data measured successively over 5–10 min (colored green-to-blue) until a maximum change in impedance is observed at the lowest frequency evaluated (10^{-1} Hz).

concentrations. Therefore, photogeneration of protons should result in a decrease in the bulk solution resistance as evidenced by a decrease in the value of the *x*-intercept of the Nyquist plot, which is measured at high frequencies. As illumination was toggled on and off, high-frequency EIS data did not exhibit a significant change in its frequency-dependent trend or the value of the *x*-intercept (Fig. S4a), suggesting that light had little-to-no influence on the bulk resistance of the cell. This observation occurred in part because for every molecule of PTS–OH, three Na^+ counterions were present, meaning that the ionic strength of the cell in the dark was inherently quite large and that small photoinduced increases in proton concentration, and therefore decreases in bulk solution resistance, would be difficult to measure. Moreover, the bulk resistance of the FTO electrodes likely dominated the total series resistance of the circuit.

Diffuse-layer capacitance changes in an opposite manner than bulk solution resistance when protons are photogenerated. However, similar to measurements of the bulk resistance, the large ionic strength inherent to these aqueous solutions precluded significant changes in the capacitance of the diffuse layer. Moreover, the capacitance of the double layer is dominated by the smaller of the capacitances of the diffuse layer and the compact layer, and over most potentials is dominated by the compact layer, which should be relatively unaffected by photogenerated protons.

Mass-transfer-limited proton-coupled redox reactivity at the electrode|electrolyte interface will also be affected by photogenerated protons. Uniquely, this would be manifest by a change in the low-frequency impedance, which was clearly observed for photo-EIS data measured at <1 Hz. This suggests that during the ±10 mV AC sweeps, redox processes that consume or generate protons occur at the FTO electrode|electrolyte interface(s). In support of this hypothesis, a linear trend in E_{oc} values as a function of pH was observed when measured using an FTO electrode immersed in deionized water in the dark (Fig. S4b). Because of this observation, we also examined the influence that light, concentrations of PTS–OH, and pH had on V_{oc} values by performing chronopotentiometry measurements (Figs. 3 and S3) in alternation with photo-EIS measurements (Figs. 2 and S3). Unlike photo-EIS measurements that probe species distributions and dynamics across the entire cell, measurements of V_{oc} values only report on phenomena that result in changes in local species concentration at or near the electrode|electrolyte interface, and any differences in the electric potential between the electrodes across the bulk solution, which we expect to be negligible. Illumination of aqueous solutions of PTS–OH resulted in non-zero values of V_{oc} (Fig. 3a), suggestive of a localized photoinduced change in pH. E_{oc} values in the dark were often non-zero (Fig. 3), presumably due to the lack of a redox couple to equilibrate with each electrode and form a well-defined potential that was identical at each electrode.

When ultrapure water in the absence of exogeneous redox couple was used instead of deionized water, trends in E_{oc} values as a function of pH, and photo-EIS data over time, were no longer monotonic (Fig. S4c). Thus, we hypothesize that impurities in the deionized water may be responsible for transducing changes in proton concentration into electronic signals. To evaluate this hypothesis, we measured the pH dependence of FTO electrodes immersed in ultrapure water containing exogenous 1 μM Fe(III/II) redox couple. A clear pH dependence on E_{oc} values was observed (Fig. S4d), and that translated to measurements using that same electrolyte in the illuminated thin-pathlength cell containing PTS–OH where V_{oc} values varied over time in a manner that was analogous to trends observed using deionized water in the absence of exogenous Fe(III/II) (Fig. S4e).

When a solution of protonated photoacids was illuminated continuously, transient responses in photo-EIS and V_{oc} data were observed on the seconds-to-minutes timescale. Initially, transient responses for both photo-EIS and V_{oc} data occurred over the same timescale (Figs. 2 and 3): as V_{oc} values increased in magnitude, photo-EIS data exhibited a decrease in low-frequency impedance. However, at longer times, and still under continuous illumination, the magnitude of the V_{oc} values reached a maximum and then decreased toward values measured in the dark, while the photo-EIS data remained rather constant. When the direction of illumination was switched, the sign of V_{oc} values changed yet the photo-EIS response was similar, as expected for a two-electrode measurement reporting on species photogenerated based on an absorption profile that follows the Beer–Lambert law. The timescales of these observations are consistent with the average time it takes for small molecules to diffuse across the width of a 250 μm thick aqueous electrolyte, $\tau = \ell^2/D = (0.025\ \text{cm})^2/(\sim 10^{-5}\ \text{cm}^2\ \text{s}^{-1}) \approx 1$ min, and with proton transport being about an order-of-magnitude faster. Collectively, this information suggests that some excited-state proton-transfer events are irreversible and/or that proton-transfer redox reactions that consume or liberate protons at the electrode|electrolyte interfaces result in non-equilibrium conditions that ultimately also influence the electrode on which light is not initially incident.

Effects of light on Bode plots and best fits of electrochemical impedance spectroscopy data.—In order to more clearly understand the change in the low-frequency impedance under illumination, where diffusional mass-transfer impedance typically dominates,[32–35] we performed further analyses of the photo-EIS data. A Warburg circuit element is often used to model EIS data that is dominated by mass transfer. It is based on a semi-infinite linear diffusion model that follows Fick's laws of diffusion and exhibits a characteristic slope of $-1/2$ for the logarithm of the magnitude of the impedance, $|Z|$, as a function of the logarithm of the frequency, and current and potential that are 45° out-of-phase. Both of these relationships are more easily visualized in Bode plots (Fig. 4), which present the change in magnitude of impedance and the phase shift of the current

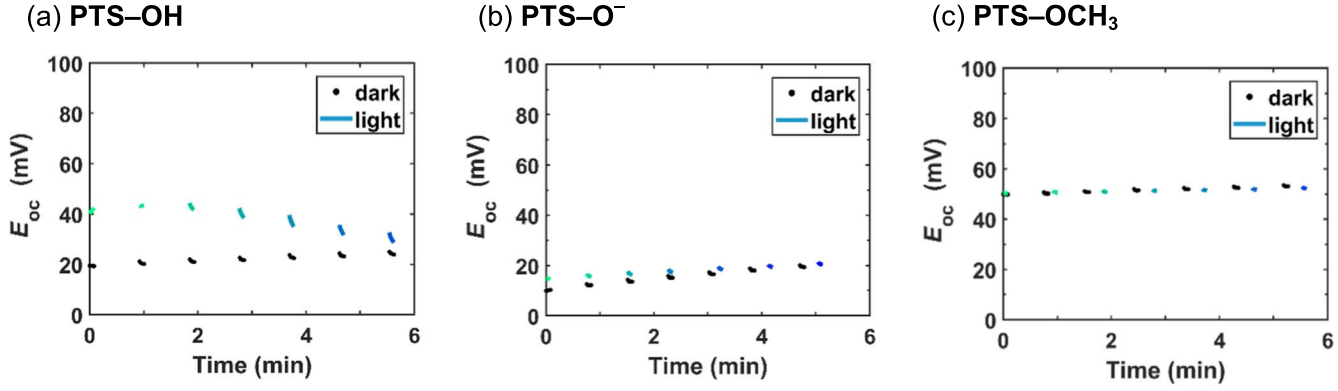

Figure 3. Open-circuit potential (E_{oc}) measured over time, and in alternation with EIS measurements (Fig. 2), for 1 mM aqueous solutions of the sodium salt of (a) PTS–OH (pH 4.2), (b) PTS–O^- (pH 9.7, from addition of approximately equimolar NaOH), and (c) PTS–OCH_3 (pH 3.7), in the dark (black) and under continuous illumination (green-to-blue) and corresponding to identical colors as for the EIS data shown in Fig. 2.

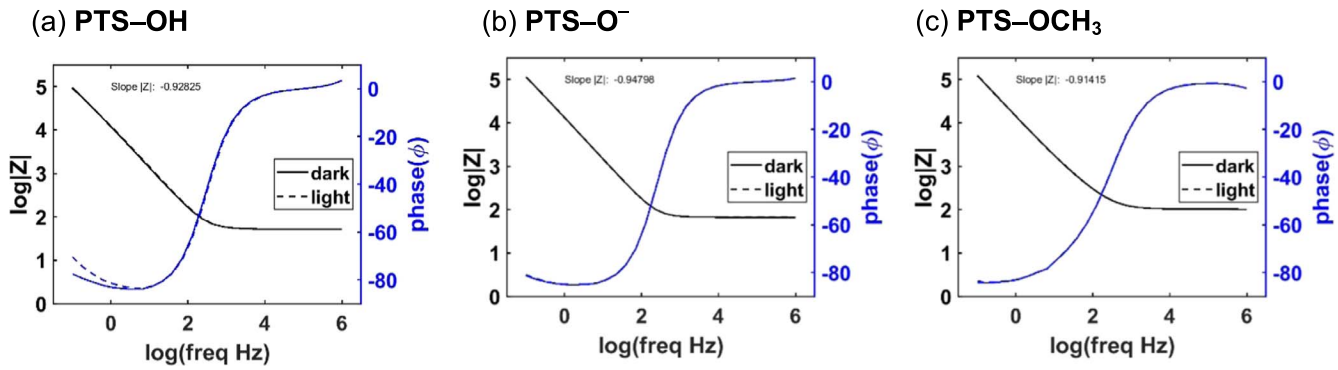

Figure 4. EIS data (from Fig. 2) plotted as Bode plots measured initially in the dark (solid) and for the maximum change under illumination (dashed) for 1 mM aqueous solutions of the sodium salt of (a) PTS–OH (pH 4.2), (b) PTS–O^- (pH 9.7, from addition of approximately equimolar NaOH), and (c) PTS–OCH_3 (pH 3.7).

−potential relationship with respect to frequency. The data clearly show trends for slope in |Z| of −1 with current and potential that are −90° out-of-phase, which are trends that are inconsistent with a Warburg impedance and instead are consistent with capacitive behavior. Thus, either the low-frequency impedance response is due to interfacial capacitance near the electrode|electrolyte interface and/or the diffusional mass-transfer process is more akin to a capacitor. At the 10^{-1} Hz frequencies analyzed, species are able to diffuse between the electrodes suggesting that the diffusion process is limited by the counter electrode and thus is not semi-infinite as required for observation of purely Warburg diffusion. Limited/confined diffusion can be modeled at low frequencies by replacing the Warburg circuit element with a parallel RC circuit[36] (Fig. 5), where R stands for the diffusional mass-transfer resistance and C stands for the capacitance of the boundary that limits diffusion. Because the boundary that limits diffusion is the counter electrode and two-electrode measurements were performed, where both electrodes are polarized and influence the measured impedance at all frequencies, the capacitance of the boundary influences the capacitive element modeling the double-layer at the working electrode, even at high frequencies. Therefore, when the diffusion layer reaches the counter electrode, no additional interfacial capacitance is introduced, and thus Warburg impedance is simplified as two resistors in series: interfacial charge-transfer resistance, R_{ct}, and diffusional mass-transfer resistance, R_{diff}. The most simplified equivalent circuit is shown in Fig. 5b, where a constant-phase element is used for the double-layer capacitance, CPE_{dl}, to represent slightly non-ideal capacitive behavior. Best fits of select data to this equivalent circuit are shown in Fig. 6 with best-fit parameters provided in Table I, and with CPE_{dl} values converted into average capacitances, $<C_{dl}>$.[37] Best-fit values for solution resistance, R_s, were determined via linear extrapolation of Nyquist plots to the real resistance x-axis. Values for CPE_{dl} and its ideality factor, a_{dl}, only differed by <2% between measurements in the dark and under continuous illumination, indicating that absorption of light did not influence capacitive processes or their degree of nonideality.

Support that photoexcitation most strongly influences interfacial charge-transfer resistance.—For both 1 mM and 10 mM PTS–OH, illumination caused the value of $R_{ct+diff}$ to decrease to less than half of its value in the dark, whereas for 10 mM PTS–OCH_3, illumination elicited insignificant changes to best-fit values. Moreover, significant changes in E_{oc} values were observed under illumination that are consistent with an approximately one-order-of-magnitude increase in proton concentration (Figs. 3, S3, and S4). Because our thin-pathlength cell does not have a membrane or a frit, E_{oc} values report on interfacial phenomena at the electrode|electrolyte interface. Collectively, these observations suggest that the observed decrease in $R_{ct+diff}$ under illumination is likely dominated by photogenerated protons at the electrode|electrolyte interface, which decrease the interfacial charge-transfer resistance for undergoing a proton-coupled charge-transfer reaction. Consistent with this hypothesis and values of $R_{ct+diff}$, interfacial charge-transfer reactions at FTO can be quite slow, even in the presence of 1 μM Fe (III/II) redox couple in ultrapure water. The exact nature of the proton-coupled charge-transfer reaction in our work is not known, but it is likely due to reversible H_2 redox or impurity redox, such as in the presence of the hexaaqua/hydroxo-Fe(III/II) redox couple. Also, the similarity of the values of $R_{ct+diff}$ for a ten-fold change in the concentration of PTS–OH (Table I) suggest that photoacids are not the predominant species that participate directly in interfacial charge-transfer at FTO. Moreover, diffusional mass-transfer resistance is not likely a major contributor to observed behavior because shapes and trends of EIS data were only moderately dependent on the thickness of the spacer in the thin-pathlength cell, as it was varied by a factor of four, from 125 μm to 500 μm (Fig. S5). Further supporting the smaller role of diffusional mass-transfer resistance to observed EIS data, changes to the FTO electrodes to convert

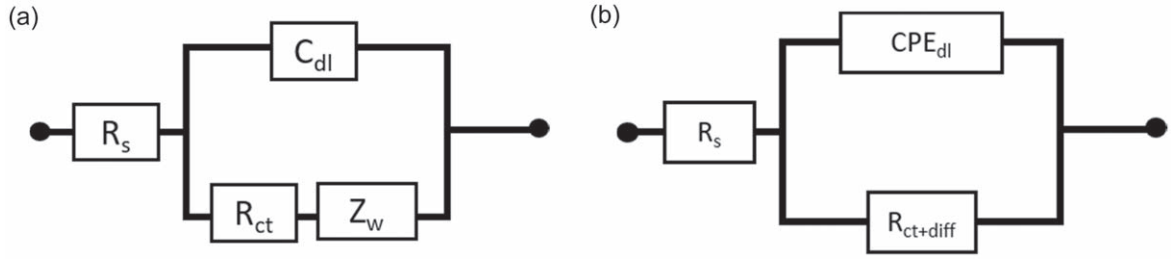

Figure 5. (a) Randles equivalent circuit for each electrode in our electrochemical cell, where R_s represents the bulk resistance, C_{dl} represents the capacitance of the double layer, R_{ct} represents the charge-transfer resistance at the electrode|electrolyte interface, and Z_w represents the diffusional Warburg impedance. (b) Simplified equivalent circuit for our electrochemical cell, where Z_w is replaced by a parallel RC (R_{diff}/C_{dl}) circuit representing limited/confined diffusion, R_s represents the bulk resistance, the capacitance, C_{dl}, is replaced with a constant-phase element (CPE_{dl}) relating to nonideal capacitive behavior, and R_{ct} is combined with the series resistor from the Warburg impedance, R_{diff}, as $R_{ct+diff}$.

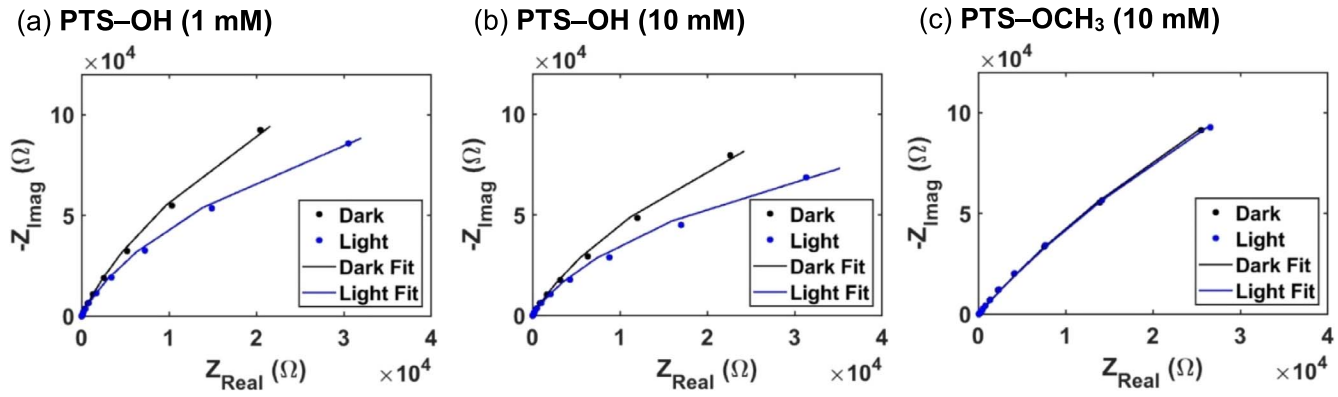

Figure 6. EIS data (dots) and best fits (lines) shown as Nyquist plots for aqueous solutions of the sodium salt of (a) 1 mM PTS–OH (pH 4.2) (from Fig. 2a), (b) 10 mM PTS–OH (pH 4.0) (from Fig. S3b), and (c) 10 mM PTS–OCH_3 (pH 4.0) (from Fig. S3h).

Table I. Best fits of photo-EIS data to the simplified equivalent circuit shown in Fig. 5b.[i)]

Condition	Circuit element	Units	In the dark	Standard deviation	Under illumination	Standard deviation
1 mM PTS–OH	R_s	Ω	51.7	*x*-intercept	51.8	*x*-intercept
	$R_{ct+diff}$	kΩ	795	0.621	294	0.146
	CPE_{dl}	Ω^{-1} s^a	15.62E-6	0.8978E-9	15.5E-6	1.117E-9
	a_{dl}		0.9344	0.5002	0.9279	0.5002
	$\langle C_{dl} \rangle$	$\mu F\ cm^{-2}$	6.43	calculated	6.01	calculated
10 mM PTS–OH	R_s	Ω	51.7	*x*-intercept	51.7	*x*-intercept
	$R_{ct+diff}$	kΩ	549	0.346	266	0.068
	CPE_{dl}	Ω^{-1} s^a	17.38E-6	1.34E-9	17.13E-6	1.598E-9
	a_{dl}		0.9151	0.5002	0.9103	0.5001
	$\langle C_{dl} \rangle$	$\mu F\ cm^{-2}$	7.39	calculated	6.86	calculated
10 mM PTS–OCH_3	R_s	Ω	85.4	*x*-intercept	86.9	*x*-intercept
	$R_{ct+diff}$	kΩ	1,253	1.353	1,238	1.269
	CPE_{dl}	Ω^{-1} s^a	15.51E-6	1.146E-9	15.27E-6	1.126E-9
	a_{dl}		0.8763	0.5001	0.8738	0.5001
	$\langle C_{dl} \rangle$	$\mu F\ cm^{-2}$	8.13	calculated	8.05	calculated

i) All parameters were adjustable except for values of the bulk resistance, R_s, which were fixed to values determined by linear extrapolation of the Nyquist plot to the real resistance *x*-axis. The geometric area used to determine $\langle C_{dl} \rangle$ values was that of the electrode|electrolyte interface (2.9 cm^2).

conditions of limited/confined diffusion with an absorbing boundary to a reflecting finite boundary did not result in a concomitant change in behavior to that of a pure capacitor expected for a reflecting finite boundary at frequencies as low as 10^{-3} Hz (Fig. S6). Lastly, if values of $R_{ct+diff}$ in the dark were due to diffusion, they would indicate a much smaller concentration of protons ($<10^{-7}$ M, pH > 7) than the concentration measured for the experimental conditions used (pH ~4 ≈ 10^{-4} M). Collectively, and unlike prior hypotheses, our data suggest that diffusion does not limit the low-frequency impedance response. While Gerischer impedance[38] due to recombination of H^+ and deprotonated ground-state photoacids could also explain the observed EIS data in the dark, with perturbations in behavior due to photogeneration of H^+ via a Beer–Lambert law absorption profile, it is more difficult to rationalize how this would lead to changes in E_{oc} under illumination that were observed experimentally.

Collectively our observations suggest that the main contributor to photoinduced changes in $R_{ct+diff}$ in our thin-pathlength electrochemical cell is an increase in local proton concentration at the electrode|electrolyte interface, which results in a decrease in the resistance for interfacial proton-coupled charge transfer. Studies are ongoing using a suite of photoacids and alternative electrode arrangements and redox reactions, coupled to transient data obtained using pulsed-laser spectroscopies, in order to better understand details of the cause of the observed AC and open-circuit photoelectrochemical responses.

Conclusions

The photoacidity of a well-known photoacid, 8-hydroxypyrene-1,3,6-trisulfonic acid, was successfully measured using alternating AC and open-circuit photoelectrochemical techniques. Electrochemical impedance spectra exhibited a significant decrease in low-frequency impedance between measurements performed in the dark and under continuous illumination for two concentrations of photoacids and several pH conditions. Control measurements performed using a methoxylated version of the photoacid, as well as the deprotonated form of the photoacid, supported that photoinduced changes in EIS data were due to changes in the concentration of protons and not due to other processes, such as excited-state electron or energy transfer or local heating. In addition, to support that a change in the concentration of protons under illumination was not manifest by a change in the series resistance of the cell, excess NaCl was added to the aqueous electrolyte, which did not result in a change in the high-frequency resistance in the dark or under continuous illumination. Alternating open-circuit potential measurements with photo-EIS measurements provided additional confirmation that illumination elicited a spatial difference in processes between the electrodes, as expected based on an absorption profile that followed the Beer–Lambert law. Alternative explanations for the observed photoresponses were considered, but the data were determined to be most consistent with a photoinduced change in proton concentration at the electrode|electrolyte interface.

Acknowledgments

The authors are grateful for financial support from the Department of Chemistry and the School of Physical Sciences at the University of California Irvine, the Gordon and Betty Moore Foundation under a Moore Inventor Fellowship (GBMF grant #5641), and Research Corporation for Science Advancement under a Cottrell Scholar Award (Award #24169). We also thank Prof. Jahan Dawlaty and Shima Haghighat for helpful discussions regarding cell design. J.G. was supported by a U.S. National Science Foundation Graduate Research Fellowship under grant number DGE-1321846.

Author Contributions

J.G. contributed to design of the experiments, prepared almost all samples, and performed almost all measurements, including subsequent analysis and interpretation of almost all data reported herein, and contributed to the preparation of the manuscript. S.L. contributed to design of a few experiments, prepared several samples, and performed some initial and final photoelectrochemical measurements, including subsequent data analysis and interpretation. T.-Y. K. prepared several samples and performed some final photoelectrochemical measurements. S.A. proposed the research and contributed to experimental design, data interpretation, and preparation of the manuscript.

ORCID

Shane Ardo https://orcid.org/0000-0001-7162-6826

References

1. N. Agmon, "Elementary steps in excited-state proton transfer." *J. Phys. Chem. A*, **109**, 13 (2005).
2. R. Simkovitch, S. Shomer, R. Gepshtein, and D. Huppert, "How fast can a proton-transfer reaction be beyond the solvent-control limit ?" *J. Phys. Chem. B*, **119**, 2253 (2015).
3. R. Simkovitch, K. Akulov, S. Shomer, M. E. Roth, D. Shabat, T. Schwartz, and D. Huppert, "Comprehensive study of ultrafast excited-state proton transfer in water and D_2O Providing the missing $RO^{-}\cdots H^{+}$ ion-pair fingerprint." *J. Phys. Chem. A*, **118**, 4425 (2014).
4. D. B. Spry, A. Goun, and M. D. Fayer, "Deprotonation Dynamics and Stokes Shift of Pyranine (HPTS)." *J. Phys. Chem. A*, **111**, 230 (2007).
5. R. Simkovitch, S. Shomer, R. Gepshtein, M. E. Roth, D. Shabat, and D. Huppert, "Comparison of the rate of excited-state proton transfer from photoacids to alcohols and water." *J. Photochem. Photobiol., A*, **277**, 90 (2014).
6. R. M. O'Donnell, R. N. Sampaio, G. Li, P. G. Johansson, C. L. Ward, and G. J. Meyer, "Photoacidic and photobasic behavior of transition metal compounds with carboxylic acid group(S)." *J. Am. Chem. Soc.*, **138**, 3891 (2016).
7. J. G. Vos, "Excited-state acid-base properties of inorganic compounds." *Polyhedron*, **11**, 2285 (1992).
8. P. J. Giordano, C. R. Bock, M. S. Wrighton, L. V. Interrante, and R. F. X. Williams, "Excited state proton transfer of a metal complex: determination of the acid dissociation constant for a metal-to-ligand charge transfer state of a ruthenium(II) complex." *J. Am. Chem. Soc.*, **99**, 3187 (1977).
9. C. Hicks, G. Ye, C. Levi, M. Gonzales, I. Rutenburg, J. Fan, R. Helmy, A. Kassis, and H. D. Gafney, "Excited-state acid–base chemistry of coordination complexes." *Coord. Chem. Rev.*, **211**, 207 (2001).
10. T. Förster, "Die pH-abhängigkeit der fluoreszenz von naphthalinderivaten." *Z. Elektrochem.*, **54**, 531 (1950).
11. Z. R. Grabowski and W. Rubaszewska, "Generalised Förster cycle. Thermodynamic and extrathermodynamic relationships between proton transfer, electron transfer and electronic excitation." *J. Chem. Soc., Faraday Trans. 1*, **73**, 11 (1977).
12. L. M. Tolbert and K. M. Solntsev, "Excited-state proton transfer: from constrained systems to "super" photoacids to superfast proton transfer." *Acc. Chem. Res.*, **35**, 19 (2002).
13. Z. Shi, P. Peng, D. Strohecker, and Y. Liao, "Long-lived photoacid based upon a photochromic reaction." *J. Am. Chem. Soc.*, **133**, 14699 (2011).
14. N. Abeyrathna and Y. Liao, "A reversible photoacid functioning in pbs buffer under visible light." *J. Am. Chem. Soc.*, **137**, 11282 (2015).
15. Y. Sheng, J. Leszczynski, A. A. Garcia, and R. Rosario, "Comprehensive theoretical study of the conversion reactions of spiropyrans : substituent and solvent effects." *J. Phys. Chem. B*, **108**, 16233 (2004).
16. J. Buback, P. Nuernberger, M. Kullmann, F. Langhojer, R. Schmidt, W. Frank, and T. Brixner, "Ring-closure and isomerization capabilities of spiropyran-derived merocyanine isomers." *J. Phys. Chem. A*, **115**, 3924 (2011).
17. H. Nakazumi, K. Maeda, S. Yagi, and T. Kitao, "Novel merocyanine dyes are converted into the spiropyran form by irradiation with visible light." *J. Chem. Soc., Chem. Commun.*, **17**, 1188 (1992).
18. A. Eilmes, "Spiropyran to merocyanine conversion: explicit vs implicit solvent modeling." *J. Phys. Chem. A*, **117**, 2629 (2013).
19. J. R. Lakowicz, *Principles of Fluorescence Spectroscopy* (Springer, New York) 3rd ed. (2006).
20. S. Haghighat, S. Ostresh, and J. M. Dawlaty, "Controlling proton conductivity with light: a scheme based on photoacid doping of materials." *J. Phys. Chem. B*, **120**, 1002 (2016).
21. S. K. Mondal, K. Sahu, S. Ghosh, P. Sen, and K. Bhattacharyya, "Excited-state proton transfer from pyranine to acetate in γ-cyclodextrin and hydroxypropyl γ-cyclodextrin." *J. Phys. Chem. A*, **110**, 13646 (2006).
22. O. F. Mohammed, J. Dreyer, B. Z. Magnes, E. Pines, and E. T. J. Nibbering, "Solvent-dependent photoacidity state of pyranine monitored by transient mid-infrared spectroscopy." *ChemPhysChem*, **6**, 625 (2005).
23. B. Finkler, C. Spies, M. Vester, F. Walte, K. Omlor, I. Riemann, M. Zimmer, F. Stracke, M. Gerhards, and G. Jung, "Highly photostable "super"-photoacids for ultrasensitive fluorescence spectroscopy." *Photochem. Photobiol. Sci.*, **13**, 548 (2014).
24. W. White, C. D. Sanborn, R. S. Reiter, D. M. Fabian, and S. Ardo, "Observation of photovoltaic action from photoacid-modified nafion due to light-driven ion transport." *J. Am. Chem. Soc.*, **139**, 11726 (2017).
25. T.-H. Tran-Thi, T. Gustavsson, C. Prayer, S. Pommeret, and J. T. Hynes, "Primary ultrafast events preceding the photoinduced proton transfer from pyranine to water." *Chem. Phys. Lett.*, **329**, 421 (2000).
26. T. Förster and S. Völker, "Kinetics of proton transfer reactions involving hydroxypyrene-trisulphonate in aqueous solution by nanosecond laser absorption spectroscopy." *Chem. Phys. Lett.*, **34**, 1 (1975).
27. C. Spies, B. Finkler, N. Acar, and G. Jung, "Solvatochromism of pyranine-derived photoacids." *Phys. Chem. Chem. Phys.*, **15**, 19893 (2013).
28. D. B. Spry, A. Goun, C. B. Bell, and M. D. Fayer, "Identification and properties of the ^1L_a and ^1L_b states of pyranine." *J. Chem. Phys.*, **125**, 144514 (2006).
29. A. A. Awasthi and P. K. Singh, "Excited-state proton transfer on the surface of a therapeutic protein, protamine." *J. Phys. Chem. B*, **121**, 10306 (2017).
30. B. G. Oscar, W. Liu, N. D. Rozanov, and C. Fang, "Ultrafast intermolecular proton transfer to a proton scavenger in an organic solvent." *Phys. Chem. Chem. Phys.*, **18**, 26151 (2016).
31. S. Luo, W. White, J. M. Cardon, and S. Ardo, "Clarification of mechanisms of protonic photovoltaic action initiated by photoexcitation of strong photoacids covalently bound to hydrated nafion cation-exchange membranes wetted by aqueous electrolytes." *Energy Environ. Sci.*, **14**, 4961 (2021).
32. A. Lasia, *Electrochemical Impedance Spectroscopy and Its Applications* (Springer, New York) (1999).
33. V. F. Lvovich, *Impedance Spectroscopy: Applications to Electrochemical and Dielectric Phenomena* (Wiley, Hoboken, New Jersey) (2012).
34. M. E. Orazem and B. Tribollet, *Electrochemical Impedance Spectroscopy* (Wiley, Hoboken, New Jersey) (2008).
35. E. Barsoukov and J. R. Macdonald, *Impedance Spectroscopy - Theory, Experiment, and Applications* (Wiley, Hoboken, New Jersey) (2005).
36. J. Bisquert, G. Garcia-Belmonte, F. Fabregat-Santiago, and P. R. Bueno, "Theoretical models for ac impedance of finite diffusion layers exhibiting low frequency dispersion." *J. Electroanal. Chem.*, **475**, 152 (1999).
37. L. Schulte, W. White, L. A. Renna, and S. Ardo, "Turning water into a protonic diode and solar cell via doping and dye sensitization." *Joule*, **5**, 2380 (2021).
38. J. Bisquert, "Theory of the impedance of electron diffusion and recombination in a thin layer." *J. Phys. Chem. B*, **106**, 325 (2002).